Climate Dynamics
https://doi.org/10.1007/s00382-019-05039-x

Relationships between convective activity in the Maritime Continent and precipitation anomalies in Southwest China during boreal summer

Yang Xia[1,2,3] · Zhaoyong Guan[1] · Yuan long[2]

Received: 11 September 2018 / Accepted: 31 October 2019

Abstract
Using the outgoing long-wave radiation (OLR) data from NOAA, the ERA-Interim reanalysis products from ECMWF, and daily observations at 756 stations provided by National Meteorological Information Center of China Meteorology Administration, we have examined the relationships of interannual variations of summer precipitation in Southwest China with the convective activity in the Maritime Continent (MC) region by employing the singular value decomposition (SVD) method and the regional climate model RegCM4.4. The first SVD mode (here after SVD1) indicates that high precipitation anomalies in Southwest China correspond to abnormally weak convective activity in northeastern MC and strong convective activity in Southwestern MC if the time-series of coefficients of SVD1 is in positive phase. When convective activity are anomalously strong in Southern MC, the anomalous divergence at 700 hPa and convergence at 200 hPa are observed over the tropical western Pacific and South China Sea. The propagation of wave energy at 700 hPa from Western Europe and the tropics provide a favorable condition for inducing more precipitation in most of Southwest China. The atmospheric water vapor transport from northern Indochina and the South China Sea to Southwest China intensifies while the western Pacific subtropical high is stronger than normal and extends more westward. All these results along with the simulations demonstrate that the summer precipitation in Southwest China is significantly affected by the convective activity over the MC region. These results above are helpful for our better understanding the role of the MC in regulating the summer climate in Southwest China.

Keywords Outgoing longwave radiation · Precipitation · Maritime Continent · Southwest China · Boreal summer

1 Introduction

The Maritime Continent (hereafter MC) is region that comprises of many islands and the surrounding shallow seas (Ramage 1968), locating in the warm pool in the Indo–Pacific sector. In this region, the air, land, and sea strongly interact with each other, and convective activity is very vigorous. Particularly, the MC is a region where the Asian monsoon interacts with Australian monsoon across the equator (e.g., Chen and Guan 2017), and the tropical Pacific interacts with the tropical Indian Ocean there via the atmospheric bridge (Alexander 2002). These interactions lead to the climate in MC to vary on multi-timescales. On the interannual time-scale, it is found that the rainfall anomalies and convective activity in the MC are strongly influenced by El Niño and Southern Oscillation (ENSO) (e.g., Ropelewski and Halpert 1987; Wang and Lin 2002; Xu and Guan 2017; Wang et al. 2017) and Indian Ocean Dipole (IOD) (Saji et al. 1999; Guan and Yamagata 2003; Jin et al. 2017; Xu et al. 2019), which have attracted wide attention in climate community since the end of the twentieth century (McBride 1998; Hamada et al. 2002; Guan et al. 2003; Hamada et al. 2008; Jiang et al. 2009).

✉ Zhaoyong Guan
guanzy@nuist.edu.cn

[1] Key Laboratory of Meteorological Disaster, Ministry of Education (KLME)/Joint International Research Laboratory of Climate and Environment Change (ILCEC)/ Collaborative Innovation Center on Forecast and Evaluation of Meteorological Disasters (CIC-FEMD), Nanjing University of Information Science and Technology, Nanjing 210044, China

[2] Meteorological Bureau of Liupanshui, Liupanshui 553000, China

[3] Guizhou Key Lab of Mountainous Climate and Resources, Guiyang 550002, China

Published online: 14 November 2019

The climate variations in MC play an important role in the interactions between East Asian and Australian monsoons. In horizontal, there are two ways in which the Asian and Australian monsoons interact with each other. The one is that the cross-equator airflows of both hemispheres interact with each other respectively via the cross equatorial exchanges of atmospheric mass and energy (e.g., Findlater 1969; Guan and Lin 1989). The other is that the East Asian and Australian monsoons interact with each other via the lateral coupling by zonal airflow at equator in MC (Chen and Guan 2017). All these two ways are determined by the variations of the large scale circulations and related to the vertical motions of the atmosphere.

The vertical circulations are also very important in interactions between Asian and Australian monsoons, especially in the influences of MC climate on the monsoon circulations. The latent heat release induced by the vigorous convective activity in MC region may strongly affect both the Walker circulation and Hadley cells (Lau and Chan 1983a, b). These vertical motions in association with the vertical circulations modulate the Asian and Australian monsoons by generating the vorticity sources including the vertically transported vorticity (Sardeshmukh and Hoskins 1988). With the onset of the East Asian summer monsoon, the tropical convective activity center gradually moves northward to Indochina, affecting the Asia-Australian monsoon circulations (e.g., Matsumoto et al. 2000; Matsumoto and Murakami 2002; Kajikawa et al. 2003; Hung and Yanai 2004; He et al. 2006), and eventually affecting the global circulations (Meehl 1987; Ropelewski and Halpert 1987; Zhang and Hagos 2009; Chen et al. 2014). For example, the released latent heat drives the atmosphere to respond, inducing both the baroclinic circulations in East Asia and the Asian jet stream to change (Chang and Lau 1982), and henceforth affecting the weather and climate in the North America (Sardeshmukh and Hoskins 1988; Yang et al. 2002; Neale and Slingo 2003). Particularly, the convective activity near the Philippines may excite the Pacific-Japan (P-J) teleconnection pattern, inducing the climate conditions in regions including Yangtze river valley, south China, Yunnan-Guizhou Plateau in China, and Japan to change anomalously (Nitta 1987; Huang and Yan 1987; Song et al. 2011; Guan and Jin 2013; Jin et al. 2013; Xia et al. 2015; Wang et al. 2016; Xu et al. 2019).

Yunan–Guizhou plateau in Southwest China (SWC) is a place in the conjunction part of the south Asian and East Asian monsoon systems (Tao and Chen 1987; Wang and Lin 2002). In recent years, SWC have experienced frequent occurrences of severe drought events. These severe events persist for a longer period than before and affect larger area in SWC than ever since, causing the huge economic losses and having high societal impacts (e.g., Bao et al. 2007; Liu et al. 2009; Qi et al. 2010; Huang et al. 2011). There are different factors that induce these severe drought events in SWC. Huang et al.(2012) reported that the energy of quasi-stationary waves anomalously propagates eastward, inducing the cold air mass to impact the SWC, and henceforth resulting in the extremely drought during autumn–winter–spring of 2009/2010. During summertime, the anomalously strong convective activity in the Philippine region can lead to western Pacific subtropical high to reinforce and extend westward anomalously, resulting in the hot and dry weather in SWC (Li et al. 2006). More than these, it is found that the descending branch of the anomalous Hadley circulation results in these severe droughts in SWC. This anomalous vertical circulation is induced by the warmer than normal sea surface temperature (SST) in tropical northwest Pacific and tropical Indian Ocean (Wang et al. 2012; Zhang et al. 2013; Feng et al. 2014).

As mentioned above, there have already been many studies to explore the anomalous atmospheric circulation and mechanisms behind for the drought events in SWC (e.g., Bao et al. 2007; Liu et al. 2009; Qi et al. 2010; Huang et al. 2011, 2012), suggesting that the MC region is probably an energy source region for the atmospheric circulation anomalies affecting the SWC. However, the impact of convective activity in MC region on climate in Southwest China along with the mechanisms behind is still far from being fully understood. Thereby, in the present study, we will reveal the relationship between convective activity in the MC and precipitation in Southwest China (SWC) and the mechanisms behind based on observational analysis and numerical experiments.

The present paper is organized as follows. We will present d brief descriptions of both data and numerical model employed after this introduction part. Then we examine the summer climatology of precipitation in Yunnan–Guizhou region. In Sect. 4, the singular value decomposition is performed of both the anomalous precipitation in SWC and outgoing longwave radiation (OLR) anomalies. The anomalous circulation patterns are revealed in Sect. 5 and the simulated results are discussed in Sect. 6. In Sect. 7, the conclusions are reached.

2 Data and method

The data used in this study includes monthly mean outgoing long-wave radiation (OLR) data (Liebmann and Smith 1996) from National Oceanic and Atmospheric Administration (NOAA), and the monthly mean ERA-Interim reanalysis (Dee et al. 2011) from European Center for Medium Range Weather Forecasts (ECMWF). There are 14 vertical levels in the ERA-Interim reanalysis with horizontal resolution of $2.5° \times 2.5°$ for both the OLR and ERA-Interim. The variables employed are winds, vertical velocity, sea level pressure (SLP), geopotential height,

mixing ratio, and etc. Daily observations at 756 stations in China are provided by National Meteorological Information Center of China Meteorological Administration (CMA). Precipitation observations at 97 stations in Southwest China during 1979–2016 without missing records are selected for the present study. Here, Southwest China is defined as the area over [97°E–112°E, 21°N–35°N], including Sichuan, Chongqing, Guizhou, Yunnan, and Guangxi. The study period covers 1979–2016. The boreal summer is defined as June–July–August.

Some statistical methods including singular value decomposition (SVD), linear regression, and so on are applied in this study (e.g., Ashok et al. 2003; Guan et al. 2003). Unless specifically stated, the climatology refers to multi-year average over June–August (1979–2016). The anomaly is defined as the difference of JJA mean value of a variable from its multi-year mean climatology. The long term trends have been removed from all data before the analysis is carried out.

Numerical experiments are conducted in this study. The regional climate model employed in the present study is RegCM4.4, which issued by the International Center of Theoretical Physics (ICTP) in 2014 (Giorgi et al. 2012, 2014). The dynamic core of RegCM4.4 is the same as that of MM5. In addition to the Biosphere–Atmosphere Transfer Scheme (BATS) (Dickinson et al. 1993) and the Community Land Model (CLM3.5) (Decker and Zeng 2009), CLM4.5 (Lawrence et al. 2011, 2012) are incorporated into this version of RegCM4.4. CLM4.5 is also the land component of the Community Earth System Model (CESM) (Hurrell et al. 2013).

3 OLR over the MC and rainfall in SWC: mean climatology

As well known, from boreal winter to summer, strong convective activity and precipitation centers in the MC seasonally shift northwards as the consecutive outbreaks of East Asian and Indian summer monsoons. From Fig. 1a, it can also be seen that there are two strong convection centers indicated by OLR in the MC. The one is located at the eastern part of the Bay of Bengal, being with value of 180 W/m^2. The other is at around the Philippines, which has a value smaller than 200 W/m^2. Corresponding to these two convective centers, maximum precipitation also occurs in the above areas with the largest value greater than 16 mm/day. Large precipitation in western Indochina and western Philippines is attributed to the combined effects of summer monsoon and orographic forcing (Chang et al. 2005). On the other hand, summer precipitation in Southwest China (Fig. 1b) displays a pattern with more precipitation in the south and less precipitation in the north. More precipitation occurs in low-topography area in Southern parts of Yunnan and Guangxi, where precipitation is greater than 10 mm/day. Precipitation less than 5 mm/day is found in northwestern Sichuan, where topography is relatively high. Meanwhile, maximum precipitation centers occur at the hilly area in Sichuan Basin and northern Chongqing, where precipitation is greater than 7 mm/day. In addition, it is interesting to see that the spatial pattern of variance of anomalous precipitation is consistent with that of precipitation; the large variability occurs over areas where the large amount of precipitation is received. In Southern Guangxi, where precipitation is large, the interannual variability exceeds 2.6 mm/day. In

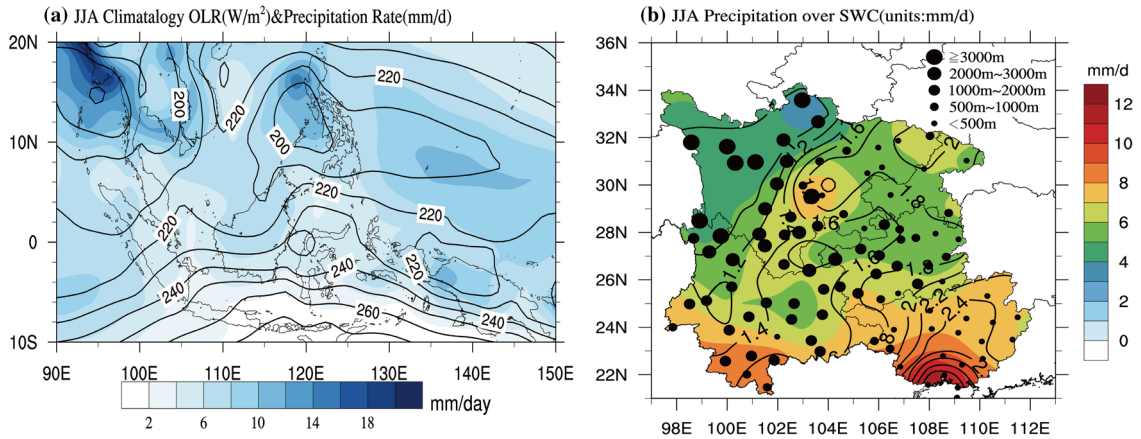

Fig. 1 Multi-year mean of June–August mean OLR (contours) and precipitation (shades) over the MC region (**a**), and multi-year mean (shades) and the variance (contours) of JJA mean precipitation in Southwest China (**b**). The altitudes and locations of observation stations in southwest China are displayed by the closed black circles in (**b**) with bigger ones for higher altitudes and the smaller for lower altitudes

contrast, the variability is smaller than 1 mm/d in western Sichuan, where precipitation is small.

4 OLR over the MC and precipitation in SWC: the SVD modes

In order to reveal the relationship between anomalies of convective activity over the MC region and precipitation in Southwest China, the SVD method is applied to MC OLR averaged over June–August during 1979–2016 and precipitation observations at 97 stations in Southwest China provided by National Meteorological Information Center of CMA. OLR over the MC region is taken as the left field, and precipitation in Southwest China as the right field. The SVD decomposition of the two fields is then performed.

The anomalous precipitation in Southwest China is significantly related to variations of OLR anomalies over the MC region. This relation can be found in Table 1. It is found that the first three leading SVD modes explain 74.43% of the total covariance, indicating that the anomalous rainfall in Southwest China is indeed significantly associated with convective activity in the MC. Importantly, the contribution of the first leading mode (SVD1) accounts for up to 34.15% of the covariance, and the correlation coefficient between time-series of expansion coefficients of the right and left fields is 0.72. This first leading mode is the most important out of the leading three, hence we will focus on the SVD1 in the following discussions.

The left and right heterogeneous correlation patterns of SVD1 along with the corresponding normalized time coefficients (Fig. 2) suggest that the OLR anomalies in northeastern and Southwestern MC vary in anti-phase relation (Fig. 2a). Positive centers are located at western Indochina and oceanic area to the east of the Philippines, respectively, with the largest correlation coefficient greater than 0.6. These positive centers correspond to strong convective centers in the summer over the MC region. Negative centers are found at some islands within the MC region, especially in the key region of the MC (Xu and Guan 2017) with the absolute value of negative correlation larger than 0.6. Meanwhile, anomalous precipitation in Southwest China varies in phase with positive correlations in almost entire region (Fig. 2b) except for a few local negative values in southeastern and western Southwest China. Two positive correlation centers are located at Sichuan Basin and Chongqing City, with the correlation coefficients of up to 0.3 and 0.4, respectively. Combined with the correlation pattern of the left field, it is clear that when convective activity is abnormally weak (strong) in northeastern MC but strong (weak) in Southwestern MC, precipitation in Southwest China is abnormally more (less). The time-series of coefficients (TC1) of left and right of SVD1 (Fig. 2c) vary in a similar way with a distinct period of 2.5 years as seen in power spectra analysis (Fig. 2d).

It should be noted that, during boreal summer, it is found that the correlation between the Southern Oscillation index (SOI) and time-series of coefficients of left field of SVD1 is 0.29, suggesting that the negative anomalies of OLR in Southwestern part of the MC may be weakly affected by the Southern oscillation. This is in agreement with McBride et al. (2003). However, as the correlation coefficient of SOI with the time-series of coefficients of right field of SVD1 is found to be 0.08, the precipitation variations in Southwestern China may not be significantly affected by the ENSO though it is closely related with the OLR anomalies in the Maritime Continent region.

5 Circulation anomalies associated with SVD1

Precipitation anomalies are usually closely related to anomalous atmospheric water vapor transport induced by anomalous circulations. In SWC, these anomalous circulations during boreal summer may be affected by circulation systems such as the monsoon trough, the Western Pacific Subtropical High (WPSH), the monsoon low pressure system in India, and the Madden–Julian Oscillation (MJO) (Wang and Li 2010; Lv et al. 2012; Yang et al. 2013; Zhang et al. 2014; Xia et al. 2016; Qian et al. 2018). In the following, we will perform the regression and correlation analyses for time series of coefficients of SVD1 to obtain the related anomalous circulation patterns and to understand the relations between variations of rainfall in SWC and those of OLR in the MC.

Table 1 Statistics of the three leading SVD modes of summer (June–August) OLR over the MC region and precipitation in Southwest China

Modes	Singular value	Covariance (%)	Expansion coefficients	Variance of left (%)	Variance of right (%)
First	18.9	34.15	0.72	20.82	10.39
Second	16.3	25.24	0.68	24.34	7.44
Third	12.6	15.04	0.71	6.94	14.33

The correlation coefficients are found to be significant if larger than 0.58 using a *t* test

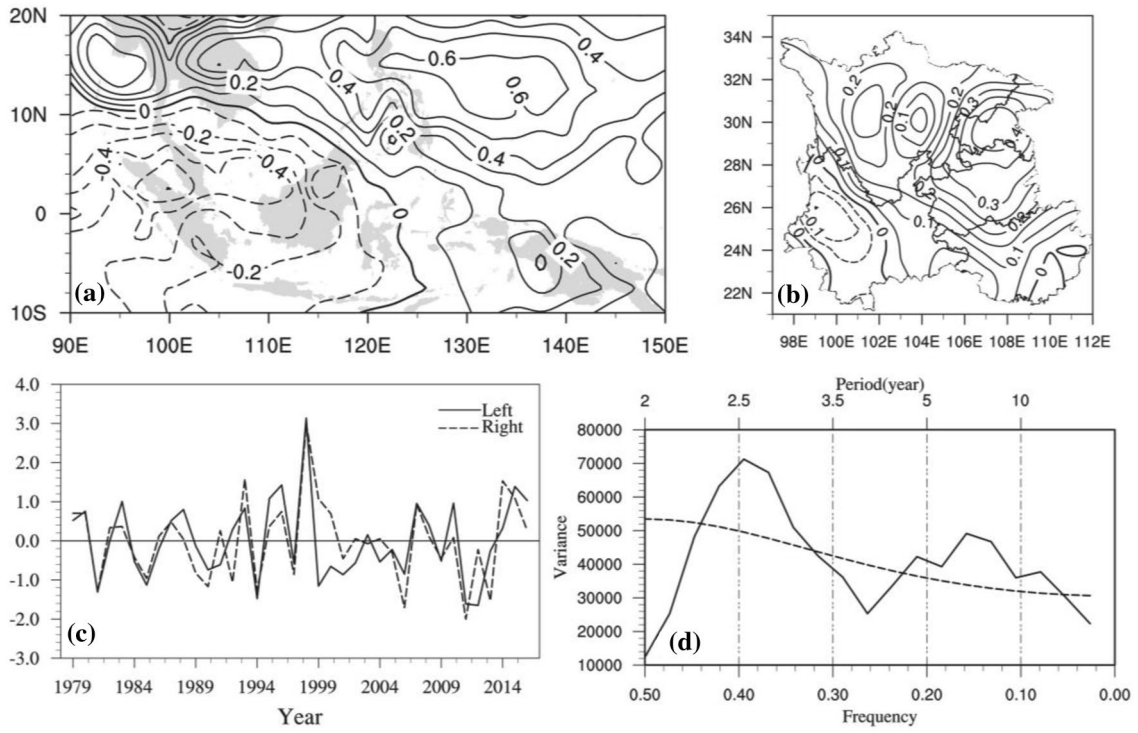

Fig. 2 Left (**a**) and right (**b**) heterogeneous correlation patterns of the first leading SVD mode for OLR over the MC region (left field) and precipitation (right field) in Southwest China, their corresponding normalized time coefficients (**c** the solid line for the left field, and the dashed line for the right field), and the power spectra of the time-series of coefficients averaged over the time-series of coefficients of left and that of right fields (**d** the solid line for the power density, and the dashed line for the red noise test at the 95% confidence level)

5.1 Water vapor transport

Precipitation in Southwest China is highly dependent on sufficient water vapor supply from the Tibetan Plateau, the Bay of Bengal, and the South China Sea (e.g., Jiang et al. 2007; Li et al. 2010). To examine the water vapor variations in Southwestern China in association with OLR in MC, we present in Fig. 3 the spatial correlations of the time-series of coefficients of the left field of SVD1 with the vertically integrated water vapor fluxes and flux divergence.

The spatial distributions of water vapor flux and flux divergence are well correspondent to precipitation anomalies (Fig. 3). Over Southwest China, the prevailing water vapor transport from the southwest to northeast intensifies to a certain degree, while more water vapor are transported to Southwest China by westerly winds to the south of the Tibetan Plateau and over northern Indochina. Due to the influence of the abnormal cyclonic circulation in the Indian Ocean and the abnormal anticyclonic circulation over northwestern Indochina, the northward water vapor transport from Indochina to Southwest China and the middle and lower reaches of Yangtze River Valley is stronger than normal. Meanwhile, northern Southwest China is also under the influence of the mid- and lower troposphere water vapor transport from the mid-latitudes to the north of the Tibetan

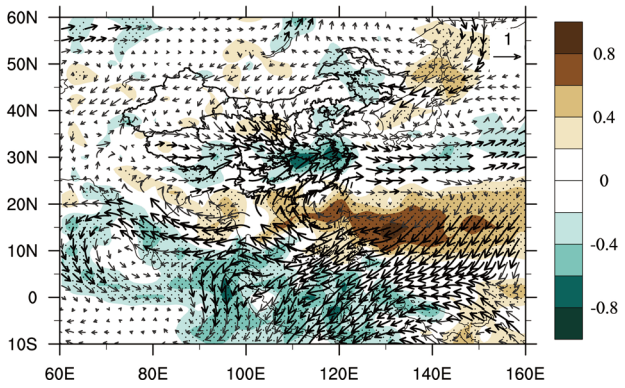

Fig. 3 Correlations of series of time coefficients of the left field of SVD1 with the water vapor flux (vectors) integrated vertically from the earth surface up to 300 hPa and with the divergence of fluxes (shades). Bold arrows and stippled areas are for values at/above the 95% confidence level using a *t* test

Plateau. Note that the water vapor flux in the Southern portion of the Southwest China gradually increases northeastward. As a result, despite the large water vapor flux over this region and South China, water vapor flux is actually divergent in these areas, which is unfavorable for precipitation. However, the northward moving warm, moist air converges

with the water vapor from the mid-latitudes in the lower troposphere. The air mass rises along the Yunnan–Guizhou plateau due to the orographic forcing, leading to the formation of precipitation.

5.2 Horizontal circulation

Since precipitation is highly relevant to local atmospheric circulation besides water vapor transport, here we presented the correlation maps of time-series of coefficients of the left field of SVD1 with horizontal circulation anomalies at different levels (700 hPa, 200 hPa) and divergent wind component (Fig. 4).

In the lower troposphere (Fig. 4a), strong convergence at 700 hPa occurs over the MC region, especially nearby Indonesia. A large abnormal anticyclonic circulation prevails over the western Pacific to the east of the Philippines, which can be explained by the apparent divergent flows originated from the central equatorial region (Gill 1980). Areas surrounding the Tibetan Plateau, including Southwest China, are under the control of this abnormal anticyclonic circulation. The above results suggest that in the summer, an intensified and westward shifted subtropical high is favorable for inland water vapor transport from the Bay of Bengal and South China Sea (Tao and Zhu 1964; Chen et al. 2011).

The anomalous circulation pattern at 200 hPain the upper troposphere looks partly opposite to that at 700 hPa (Fig. 4b). A strong convergence center is located at the eastern MC and western Pacific; a divergence center is found at the Southern Indian Ocean to the west of MC. The abnormal convergence center triggers a northeastward propagating cyclone-anticyclone-cyclone wave train to its west, which is similar to the P-J wave train. The South Asia High above the Tibetan Plateau looks to shift more eastward than normal with abnormally high intensity.

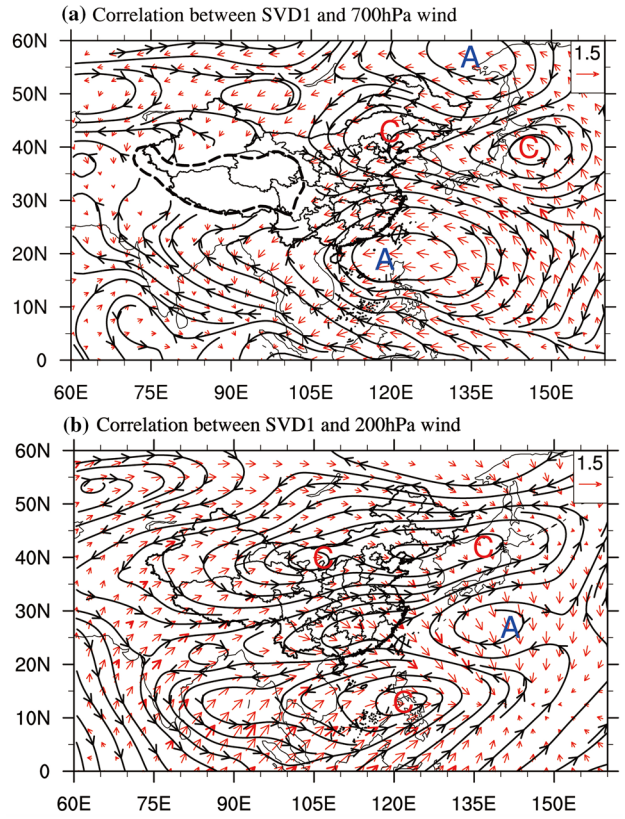

Fig. 4 Correlations of series of time coefficients of the left field of SVD1 with divergent (arrows) and rotational (streamlines) wind components at **a** 700 hPa and **b** 200 hPa. Bold arrows are for values at/above the 95% confidence level using a *t* test. The thick dashed lines at 700 hPa are for the topography higher than 3000 m

5.3 Vertical circulation

In order to reveal the possible influences of convective activity in the MC on the precipitation variations in Southwest China, the TC1-regressed vertical circulations along the slanted line across geographic points (125°E, 5°S) in the MC and (100°E, 40°N) are presented in Fig. 5.

The vertical circulations exhibit some distinct features of atmospheric motion in relation with the convective activity in the MC. It is seen from Fig. 5a that the multi-year mean vertical velocity indicates that the upward motions appear over Yunnan–Guizhou plateau between two vertical circulation centers that locate respectively at 35°N and 2°S. In the subtropics, the maximum vertical velocity greater than 8×10^{-2} Pa/s appears at around 400 hPa. This vertical motion maximum appears along with the weak downward motion within a very thin layer just above the earth surface in the MC region. However, the largest ascending motion in Southwest China occurs at 700 hPa, which is possibly associated with the orographic lifting of atmosphere in lower levels.

The abnormal circulation along the vertical cross section across the MC region and Southwest China (Fig. 5b) shows that there exists a distinct meridional circulation anomaly in the tropics, with the center located nearby (112°E, 18°N) at 500 hPa. The ascending branch of the circulation anomaly appears in the tropics and to its south, while the descending branch is located above the northern MC and southern edge of Southwest China. This pattern is well corresponding to the OLR distribution in the MC shown in the left field of the first leading SVD mode. The air rises above the southern MC, turns northward in the upper layer of troposphere, and bifurcates into two branches at 200 hPa over the central to northern MC. One branch is accompanied by the descending branch of the abnormal meridional circulation and reaches the lower levels before it turns northerly and returns to the tropics, forming a complete meridional circulation. The other branch merges into the ascending flow to the east of

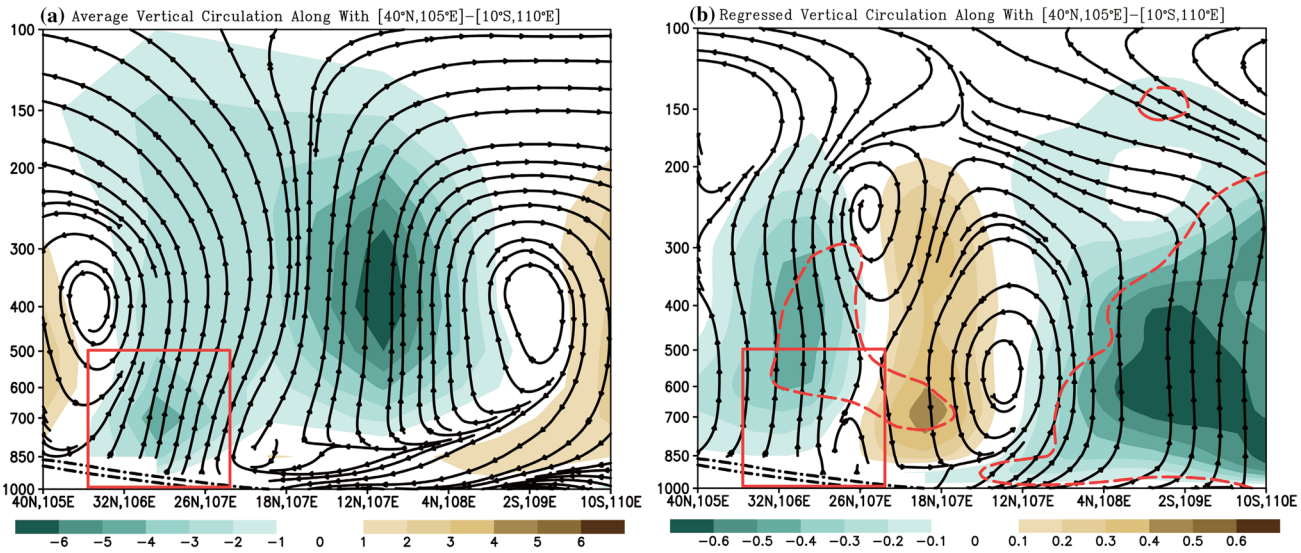

Fig. 5 Vertical circulation along the slanted line from (125°E, 5°S) to (100°E, 40°N) for summertime multi-year mean climatology (**a**) and the anomalous vertical circulation as obtained by regressed it upon time-series of coefficients of the left field of SVD1 (**b**). Streamlines are for the circulations whereas the shaded contours for vertical velocity in unit of 10^{-2} Pa/s. Black dot-dashed lines are for topography and the red rectangular frame for Southwest China. Red dashed lines indicate the values are significant at/above the 95% confidence level using an *F* test

the Tibetan Plateau. As a result, most of Southwest China is under the control of abnormal ascending motions. Compared to multi-year average vertical circulation, it can be found that when convective activity is stronger than normal over southern MC, i.e. when the strong convection center shifts to the south of its normal position, the descending motion in southern MC turns to abnormally strong ascending motion. As a result, the descending branch of the Hardly Cell shifts southward than normal and reaches South China, leading to significant weakening of ascending motions over some summer monsoon region. Meanwhile, descending motions greatly intensify over Southwest China, resulting in large increases in precipitation over the Yangtze River valley and Southwest China.

5.4 Wave activity flux

Several studies (Duan et al. 2007; Xia et al. 2015) have pointed out that the circulation anomalies affecting precipitation in late autumn, early winter, and during the rainy season are possibly associated with the propagation of quasi-stationary waves triggered by tropical forcing. In order to clarify the mechanism for the generation and maintenance of the abnormal circulation over Southwest China and its relationship with the Rossby wave propagations in westerlies, here we presented geopotential height anomalies that relates to SVD1 and corresponding wave activity flux (Takaya and Nakamura 1997; Takaya 2001; Huang et al. 2013) at various levels (700 hPa, 200 hPa) of the troposphere (Fig. 6).

It is found that the circulations at 700 hPa in southern China can be affected by the wave energy dispersed from both the tropical MC region and the mid- latitudes. In the mid-latitudes, the geopotential height anomaly in the lower troposphere at 700 hPa regressed on the time coefficients of the left field of SVD1 (Fig. 6a) shows a negative–positive–negative pattern from West Europe to the mid- and high-latitudes of northeastern Asia. Negative anomalies are located above West Europe and northern China, whereas positive anomalies are found in northern central and northeastern Asia. Meanwhile, negative geopotential height anomalies can also be found over the western Central Siberian Plateau, while positive anomalies are located at the northwestern Pacific including southeastern Asia. The above features further indicate that the western Pacific subtropical high is stronger and westward-shifted than normal. The T–N flux shows that the wave energy propagates downstream from the mid- and high-latitudes of West Europe, and converges in central Asia, producing and maintaining the positive geopotential height anomalies there. The wave energy is then dispersed to northeastern Asia through the Central Siberian Plateau, and plays a critical role to maintain the positive geopotential height anomaly in northwestern Asia. In the tropical region, the wave energy propagates northward, and finally converges with the energy from the north to affect (Fig. 6a). The convergence of T–N flux above China is favorable for the maintenance of perturbation of geopotential height to the east of the Tibetan Plateau.

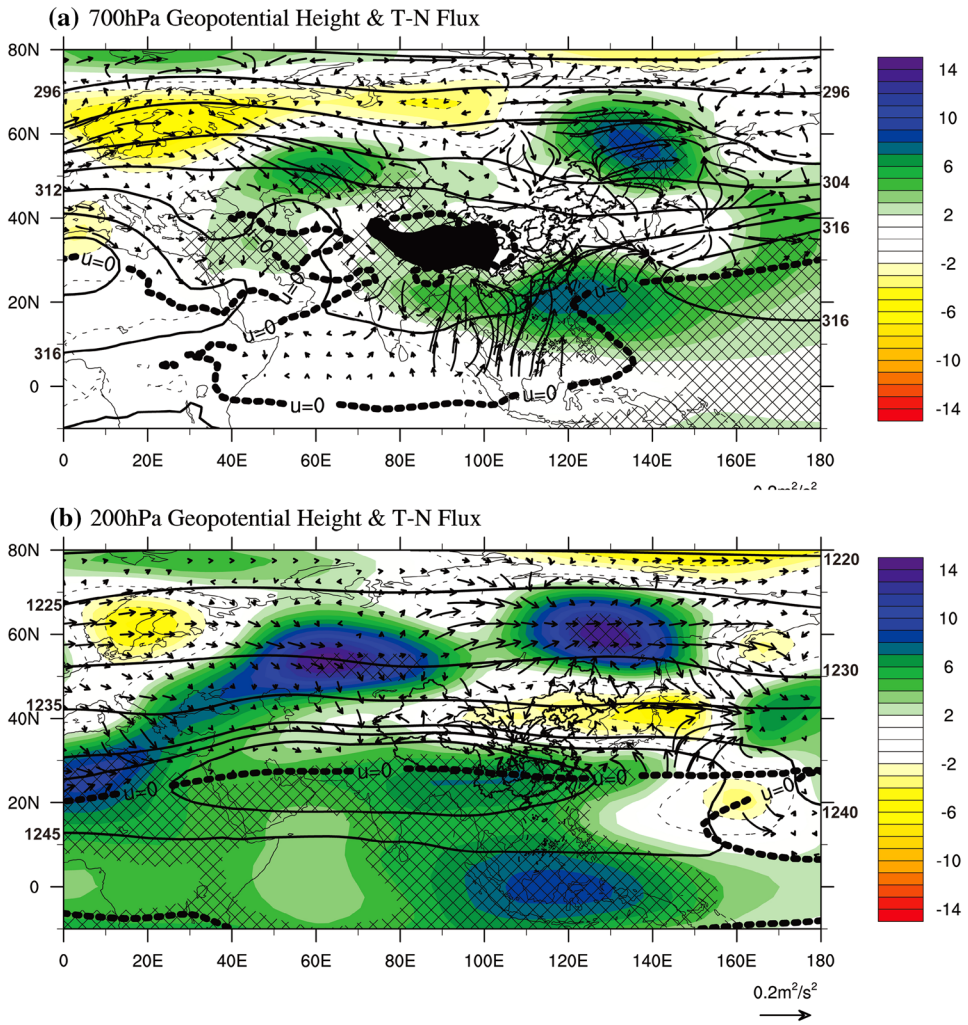

Fig. 6 The TC1-regressed anomalous geopotential height (shaded, 10gpm) and the mean climatology (black solid contours, 10gpm) over Eurasia in boreal summer, and regressed T–N flux (vectors) with unit in m^2/s^2 at 700 hPa (**a**) and 200 hPa (**b**). The thick dashed line is for zero zonal wind of mean climatology. The cross-slashed areas are for the anomalous geoptential heights at/above the 95% confidence level using an *F* test

In the upper troposphere (Fig. 6b), the geopotential height anomaly distribution is similar to that in the lower troposphere. Negative anomalies are found in West Europe and northeastern China, while positive anomalies are located in central and northeastern Asia. This result indicates that the abnormal system has a quasi-barotropic structure. However, the waver energy that affects China and East Asia is originated only from the westerlies in mid-latitudes.

6 Numerical experiments

Local changes are usually small for monthly mean circulation, which explains why diabatic heating anomaly is often balanced by dynamic heating. The analyses in previous sections indicate that precipitation anomaly in Southwest China, which is induced by abnormal convective activity over the MC region, is associated with the vertical motion of the abnormal meridional circulation in the troposphere. Here we perform the numerical experiments to examine if the anomalous thermal forcing can affect the precipitation over Southwestern China.

6.1 Experiment design

RegCM4.4 is a well known regional climate model which is widely used to simulate the regional climate variations (Giorgi et al. 2012, 2014). Here, we employ this model to simulate the circulation changes in association with the thermal forcing in the MC. In the tropics, the strong convection is usually associated with the warmer SSTA except in the some areas where the decent of air dominates. This OLR–SST relation can be examined by the correlations between anomalous OLR and SSTA in the MC region (Fig. 7a). The negative correlations between OLR and SSTA are observed in most of the MC except in a small area in the northeastern MC where the correlation is positive. This pattern looks similar to the OLR pattern of SVD1 (Fig. 2a). In fact, the SVD1-related SST anomalies in the MC are dominantly positive, suggesting that the lower OLR is induced

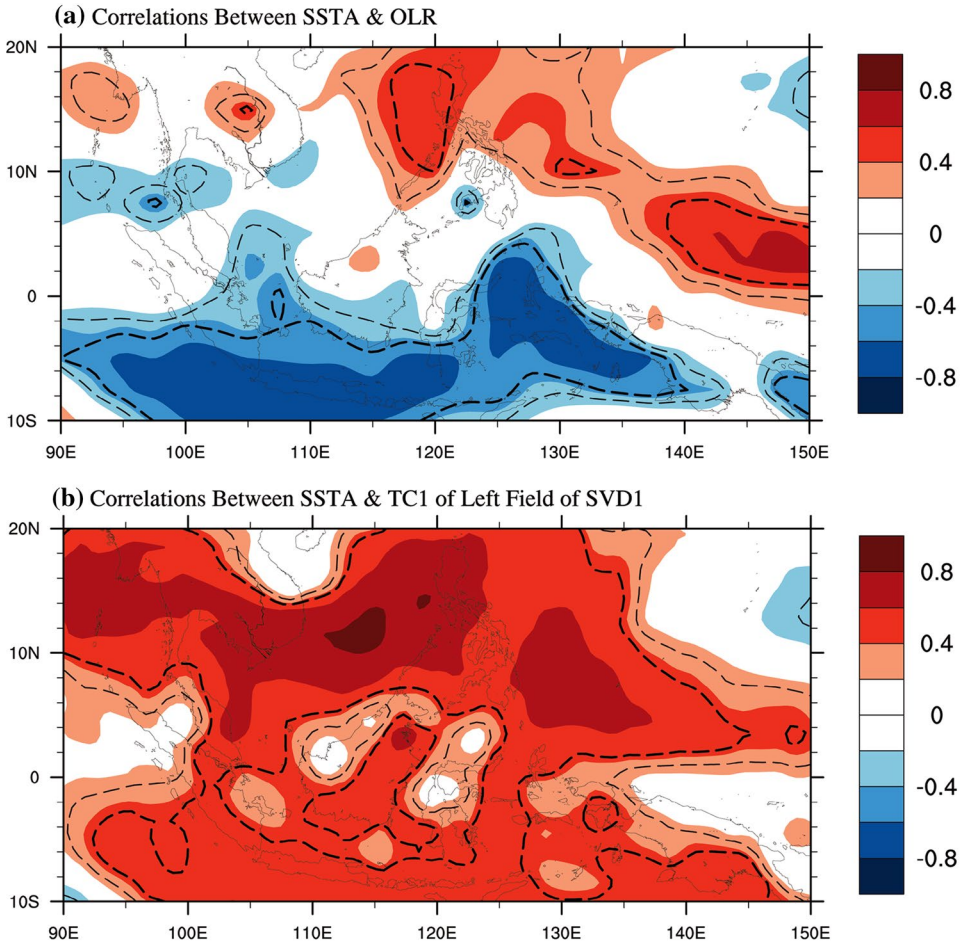

Fig. 7 Correlations (shaded) of SSTA with **a** OLR anomalies over the MC region in boreal summer (June–August), and with **b** TC1 of left field of SVD1. The areas circled with thickest (thinner) dashed black iso-lines are for correlations values at/above 99% (90%) confidence level using a *t* test. The thinnest grey lines are for outlines of both lands and islands

by the warmer SSTA in Southwestern part of the MC while the larger OLR is also induced by the warmer SSTA in the northeastern part of the MC where the downward motion dominates (Fig. 7b). Therefore, it is reasonable for us to use the idealized uniform SSTA in the MC to force the atmosphere to examine if there are impacts of thermal forcing in the MC on precipitation in Southwest China. Note that only are the SST anomalies in the key area of the MC (Xu and Guan 2017) superimposed on the SST climatology.

The model domain covers [43°E–167°E, 26.5°S–56.3°N] with the center at (105°E, 20°N) (Fig. 8). There are 171×220 (zonal × meridional) grid points in the horizontal with grid interval of 60 km in the model domain. In the vertical there are 18 levels and the model top is at 50 hPa. In this simulation, the time step is set to 100 s. The initial and boundary conditions are derived from the ERA-Interim reanalysis products of ECMWF. The ERA-Interim gridded data has a resolution of 1.5° × 1.5° (lon. × lat.). Important physical schemes include the NCAR CCM3 radiation scheme (Kiehl et al. 1993), the Zeng scheme for sea surface flux calculation (Zeng et al. 1998), the SUBEX scheme for large-scale precipitation (Pal et al. 2000), the Grell cumulus scheme

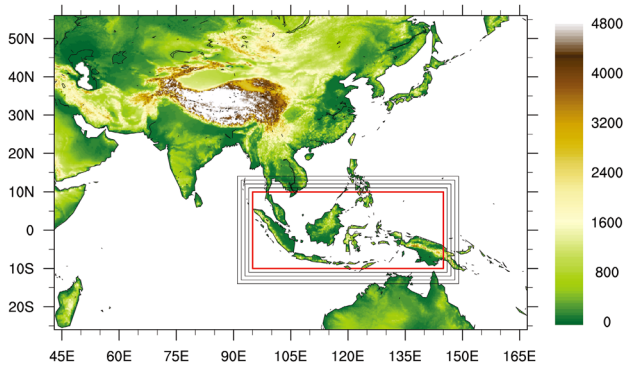

Fig. 8 The model domain (outmost frame) and topography (shades, in m). The red rectangular frame indicates the key area of the MC region and the area enclosed by grey solid line shows the buffer zone for SST variation

that is based on the Fritsch-Chappell closure (Fritsch and Chappell 1980; Grell 1993), the Holtslag planetary boundary scheme (Holtslag et al. 1990), and the CLM3.5 surface scheme (Decker and Zeng 2009). The SRES A1B scenario was taken for green house gas release (Hasumi and Emori 2004). SST is extracted from the NCEP/NCAR Optimum

Interpolation Sea Surface Temperature (OISST) (Reynolds et al. 2002).

The model was initialized at 0000 UTC 1 May and the integration ended at 0000 UTC 1 September of each individual year. In climate simulation, either long-term integration or large ensemble simulation is required in order to obtain statistically significant results of the interannual atmospheric variability in response to tropical SST (Kumar and Hoerling 1995; Sardeshmukh et al. 2000). Therefore, in this study, a 31-member ensemble simulation with different initial conditions (1982–2012) was conducted. The first month (May) was taken as spin-up time and excluded from analysis. Five experiments were conducted. They are: (1) the control experiment (CTRL): only seasonal variation is retained in SST, which is then used in the 31-member ensemble simulation. The ensemble mean of the 31 members is averaged over the summer for further analysis; (2) the positive SSTA experiment (SSTH1): same as CTRL, except that SST over the MC is increased by 1 °C from May 1st to September 1st. A buffer zone of 5° lat. and lon. is set to avoid abrupt SST change along the boundaries of the MC region (Fig. 8); (3) the negative SSTA experiment (SSTL1): the same as in SSTH1 except that SST over the MC is decreased by 1 °C; (4) the positive SSTA experiment (SSTH2): the same as SSTH1, except that SST over the MC is increased by 2 °C; (5) the negative SSTA experiment (SSTL2): the same as SSTH1 except that SST over the MC is decreased by 2 °C.

6.2 Experiment results

The spatial pattern of summer precipitation and its standard deviation simulated by CTRL (Fig. 9a) is looks reasonable in as compared to observations (Fig. 1b); less precipitation is in the south and more precipitation in the north over Southwest China. The maximum precipitation center nearby Sichuan Basin is also realistically simulated although the precipitation intensity is overestimated. At the same time, it is seen from Fig. 9a that the place where the standard deviation is large is just the place where precipitation is large. This simulated feature of precipitation variability is consistent with the observations as seen in Fig. 1b, suggesting that simulated overall features are roughly realistic.

In order to examine the impact of SST anomalies in the MC on precipitation anomalies in Southwest China, mean composite differences in the simulations between positive and negative SST anomaly cases, i.e. SSTH1 vs. SSTL1 (Fig. 9b) and SSTH2 vs. SSTL2 (Fig. 9c), are analyzed. Results indicate that when SST in the MC region is higher than normal, i.e. convective activity is abnormally strong in the south and weak in the north, stronger than normal southerly winds prevail above Southwest China. Divergence occurs in the southeastern part of Southwest China, while convergence appears in central and northern part, leading to abnormally high precipitation in most areas of Southwest China except the southern edge where precipitation decreases. In general, the simulation results are consistent with that of statistical analysis (Fig. 2b), suggesting that convective activity over the MC region can have significant impacts on the precipitation in Southwest China.

7 Conclusions

Based on the above analyses, we find that there are close relationships between the precipitation in Southwestern China and the convective activity in the Maritime Continent region. Main results are summarized as follows.

Climatologically, three strong convective centers are respectively observed in regions nearby Indochina, the southern Philippines, and northwestern New Guinea in the summer over the MC region. Among the three centers, OLR over the ocean nearby Indochina is lower than 180 W/m^2. Large precipitation centers correspond to the three convective centers. In Southwest China, more precipitation occurs in the south than in the north. The large precipitation centers appear in southern Yunnan and Guangxi while a low precipitation center appears in northwestern Sichuan. The maximum precipitation center is observed in Sichuan Basin. The interannual variability of precipitation is larger over areas where more precipitation occurs.

The summer precipitation anomalies in Southwest China are found to be closely associated with interannual variations of convective activity over the MC region. The first leading SVD mode exhibits a feature of abnormally low (high) OLR in the south and high (low) OLR in the north of the MC region, which correspond to stronger (weaker) than normal convective activity in the south and weaker (stronger) than normal convective activity in the north. The time-series of coefficients of SVD1 reveals that these precipitation anomalies vacillate between the positive and negative phases with a period of 2.5 years.

The precipitation variations in Southwest China are connected to OLR changes in the MC via anomalous transport of water vapor. When in the positive (negative) phase of TC1, the water vapor transport from northern Indochina and the South China Sea to Southwest China intensifies (weakens), leading to abnormal water vapor convergence (divergence) and higher (lower) than normal precipitation in Southwest China.

The anomalous circulations over southwest China and convective activity in the MC can also be linked by the anomalous circulations. In the positive of TC1, the significant abnormal meridional-vertical circulations are well defined between the MC region and Southwest China. Strong convective activity over the MC region corresponds to convergence in the lower troposphere and divergence in

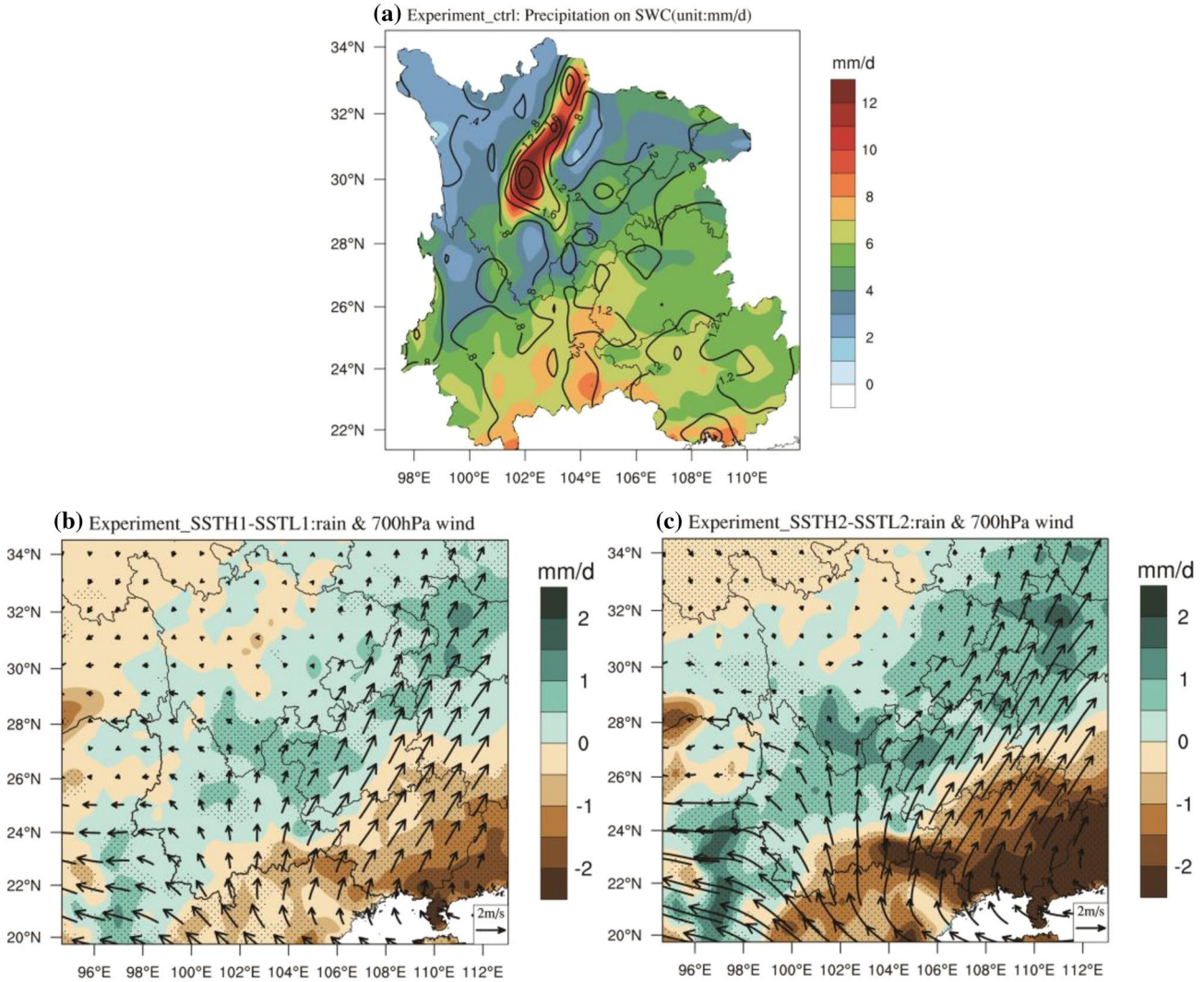

Fig. 9 Simulated summer mean climatology of precipitation (shaded) in unit of mm/day and standard deviation of precipitation (contours) with interval of 0.4 mm (**a**), mean composite differences of precipitation in mm/d and winds at 700 hPa between the positive SSTA (SSTH1) and negative SSTA (SSTL1) cases of the ensemble experiments (**b**), and those between SSTH2 and SSTL2 cases (**c**) in Southwest China. The cross-hatched areas show values of precipitation anomalies significant at and above the 95% confidence level using a *t* test

the upper troposphere, and large ascending motion. The northern MC is under the control of descending motion with less precipitation. In Southwest China, the subtropical high intensifies and shifts westward than normal due to the influence of the abnormal divergence in the upper troposphere over the tropical western Pacific. As a result, ascending motion intensifies abnormally over Southwest China. In addition, the wave energy triggered by convective anomalies over the MC region propagates to China, where it merges with the energy dispersed downstream from mid- and high-latitudes. Together with anomalous convergence (divergence) of water vapor in Southwest China, these anomalous circulations between the MC and southwest China are favorable for the intensification and westward shift of the subtropical high, while the South Asia High also intensifies and shifts eastward, eventually inducing significant anomalous precipitation over Southwest China.

The strong convective activity is strongly related to the SSTA forcing in the key area of the MC region. By employing the regional climate model RegCM4.4, five sets of ensemble experiments have be conducted to examine whether the thermal forcing in the MC can affect the precipitation in Southwest China or not. The simulated results do show that when SST in the key area of the MC region overall is higher than normal, i.e. convective activity is abnormally strong in the south, stronger than normal southerly winds prevail above Southwest China, leading to abnormally more precipitation in most area of Southwest China.

It should be stressed that the purpose of this work is to examine the influences of SSTA in the Key region of the MC (Xu et al. 2019) on the rainfall anomalies in Southwest China. Whether the SSTA in the MC and rainfall in Southwest China are influenced by ENSO or not is not discussed. The simultaneous influence of ENSO on the rainfall anomalies in Southwest China is an interesting topic, which deserves more detailed future investigations. Moreover, the SSTA used in simulations are confined in the key area of the MC. If the SSTA in the whole MC domain are consider in the numerical experiments, what do the circulation variations look like? This also needs to be examined in the near future.

Acknowledgements This work is supported by the project of Natural Science Foundation of China (No. 41330425). NCEP/NCAR re-analyses are downloaded from the website of NOAA Earth System Research Laboratory (http://www.esrl.noaa.gov/). NOAA_OI_SST_V2 data provided by the NOAA/OAR/ESRL PSD, Boulder, Colorado, USA, from their Web site at https://www.esrl.noaa.gov/psd/. Figures are plotted using both Grads and NCL software packages.

References

Alexander AM (2002) The atmospheric bridge: the influence of ENSO teleconnections on air-sea interaction over the global oceans. J Clim 15(16):2205–2231

Ashok KZ, Guan Z, Yamagata T (2003) A look at the relationship between the ENSO and the Indian Ocean dipole. J Meteorol Soc Jpn 81(1):41–56

Bao Y, Kang Z, Jin R et al (2007) Analysis of floods and droughts in Chongqing and East Sichuan. Meteorol Monthly 33(5):85–93 **(Chinese)**

Chang CP, Lau KM (1982) Short-term planetary-scale interactions over the tropics and midlatitude during northern winter. Part I, Contrasts between active and inactive periods. Mon Weather Rev 110(8):1666–1672

Chang CP, Harr PA, Chen HJ (2005) Synoptic Disturbances over the Equatorial South China Sea and Western Maritime Continent during Boreal Winter. Mon Weather Rev 133:489–503

Chen W, Guan Z (2017) A joint monsoon index for East Asian- Australian monsoons during boreal summer. Atmos Sci Lett 18:403–408

Chen Y, Li Y, Qi D (2011) Variations of South Asia High and West Pacific Subtropical High and their relationships with precipitation. Plateau Meteor 30(5):1148–1157 **(Chinese)**

Chen Z, Wen Z, Wu R et al (2014) Influence of two types of El Niño on the East Asian climate during boreal summer: a numerical study. Clim Dyn 43(1):469–481

Decker M, Zeng X (2009) Impact of modified Richards equation on global soil moisture simulation in the Community Land Model (CLM3. 5). J Adv Model Earth Syst 1(3):1–22

Dee DP, Uppala SM, Simmons AJ et al (2011) The ERA-Interim reanalysis: configuration and performance of the data assimilation system. Q J R Meteorol Soc 137(656):553–597

Dickinson RE, Hendersonsellers A, Kennedy J(1993) Biosphere-atmosphere transfer scheme (BATS) version 1e as coupled to the NCAR community climate model. NCAR Tech. Note

Duan C, Zhu Y, You W (2007) Characteristic and formation cause of drought and flood in Yunnan province rainy season. Plateau Meteor 26(2):402–408 **(Chinese)**

Feng L, Li T, Yu W (2014) Cause of severe droughts in Southwest China during 1951–2010. Clim Dyn 43:7–8

Findlater J (1969) A major low-level air currents near the Indian Ocean during the northern summer. Q J R Meteorol Soc 95(2):362–380

Fritsch JM, Chappell CF (1980) Numerical prediction of convectively driven mesoscale pressure systems. Part I. Convective parameterization. J Atmos Sci 37(3):1722–1733

Gill AE (1980) Some simple solutions for heat-induced tropical circulation. Q J R Meteorol Soc 106(449):447–462

Giorgi F, Coppola E, Solmon F et al (2012) RegCM4: model description and preliminary tests over multiple CORDEX domains. Clim Res 52(1):7–29

Giorgi F, Coppola E, Raffaele F et al (2014) Changes in extremes and hydroclimatic regimes in the CREMA ensemble projections. Clim Change 125(1):39–51

Grell G (1993) Prognostic evaluation of assumptions used by cumulus parameterizations. Mon Weather Rev 121(3):764–787

Guan Z, Jin D (2013) Two opposite extreme events in seasonal mean winter rainfall over East China during the past three decades. Atmos Ocean Sci Lett 6(5):240–247

Guan Z, Lin C (1989) Some characteristics of circulation over middle and low latitudes of eastern hemisphere during anomalous droughts and floods in 1981 and 1983. Sci Meteorol Sin 9(1):80–85 **(Chinese)**

Guan Z, Yamagata T (2003) The unusual summer of 1994 in East Asia, IOD teleconnections. Geophys Res Lett 30(10):1544

Guan Z, Ashok K, Yamagata T (2003) Summertime response of the tropical atmosphere to the Indian Ocean sea surface temperature anomalies. J Meteorol Soc Jpn 81(3):533–561

Hamada J, Yamanaka M, Matsumoto J et al (2002) Spatial and temporal variations of the rainy season over Indonesia and their link to ENSO. J Meteorol Soc Jpn 80(2):285–310

Hamada J, Yamanaka M, Mori S et al (2008) Differences of rainfall characteristics between coastal and interior areas of central western Sumatera, Indonesia. J Meteorol Soc Jpn 86(5):593–611

Hasumi H, Emori S (eds) (2004) K-1 coupled model (MIROC) description, K-1 technical report 1, Center for Climate System Research, University of Tokyo

He J, Wen M, Ding Y et al (2006) Possible Mechanism of The Effect of Convection over Asian-Australian "Land Bridge" on the East Asian Summer Monsoon Onset. Sci China Earth Sci 49(11):1223–1232 **(Chinese)**

Holtslag A, Bruijn E, Pan HL (1990) A high resolution air mass transformation model for short-range weather forecasting. Mon Weather Rev 118:1561–1575

Huang R, Yan B (1987) The physical effects of topography and heat sources on the formation and maintenance of the summer monsoon over Asia. Adv Atmos Sci 4(1):13–23

Huang H, Li Q, Gao Y et al (2011) Diagnosis of the Severe Drought in Autumn/Winter 2009-2010 in Yunnan Province. Trop Geogr 31(1):28–33 **(Chinese)**

Huang R, Liu Y, Wang L (2012) Analyses of the causes of severe drought occurring in Southwest China from the fall of 2009 to the spring of 2010. Chin J Atmos Sci 36(3):443–457 **(Chinese)**

Huang X, Guan Z, Dai Z et al (2013) A further look at the interannual variations of East Asian trough intensity and their impacts on winter climate of China. Acta Meteorol Sin 71(3):416–428 **(Chinese)**

Hung CW, Yanai M (2004) Factors contributing to the onset of the Australian summer monsoon. Q J R Meteorol Soc 130(597):739–761

Hurrell JW, Holland MM, Gent PR et al (2013) The community earth system model, a framework for collaborative research. Bull Am Meteorol Soc 94(9):1339–1360

Jiang X, Li Y, Li C et al (2007) Characteristics of summer water vapor transportation in Sichuan Basin and its relationship with regional drought and flood. Plateau Meteor 26(3):476–484 **(Chinese)**

Jiang L, Guan Z, Lu C et al (2009) Interdecadal characters of relationships of the interannual variability of East Asian Summer Monsoon with IOD and ENSO. J Nanjing Inst Meteorol 32(1):32–44 **(Chinese)**

Jin D, Guan Z, Tang W (2013) The extreme drought event during winter–spring of 2011 in east china, combined influences of teleconnection in mid- high- latitudes and thermal forcing in maritime continent region. J Clim 26(20):8210–8222

Jin D, Guan Z, Huo L et al (2017) Possible impacts of spring sea surface temperature anomalies over South Indian Ocean on summer rainfall in Guangdong-Guangxi region of China. Clim Dyn 49:3075–3090

Kajikawa Y, Yasunari T, Kawamura R (2003) The role of the local Hadley circulation over the western Pacific on the zonally asymmetric anomalies over the Indian Ocean. J Meteorol Soc Jpn 81(2):259–276

Kiehl J, Hack J, Bonan G et al (1993) Description of the NCAR community climate model (CCM3). NCAR Tech Note 11(2):55–60

Kumar A, Hoerling MP (1995) Prospects and limitations of seasonal atmospheric GCM predictions. Bull Am Meteorol Soc 76(3):335–345

Lau KM, Chan PH (1983a) Short-term climate variability and atmospheric teleconnections from satellite-observed outgoing longwave radiation. Part I: simultaneous relationships. J Atmos Sci 40(12):2735–2750

Lau KM, Chan PH (1983b) Short–term climate variability and atmospheric teleconnections from satellite-observed outgoing longwave radiation, Part II: lagged correlations. J Atmos Sci 40(12):2735–2750

Lawrence DM, Oleson KW, Flanner MG et al (2011) Parameterization improvements and functional and structural advances in version 4 of the Community Land Model. J Adv Model Earth Syst 3(1):265–375

Lawrence DM, Oleson KW, Flanner MG et al (2012) The CCSM4 land simulation, 1850–2005: assessment of surface climate and new capabilities. J Clim 25(7):2240–2260

Li YH, Xu HM, Liu D (2006) Feature of the extremely severe drought in the east of Southwest China and anomalies of atmospheric circulation in summer 2006. Acta Meteorol Sin 67(1):122–132 **(Chinese)**

Li X, Liang W, Wen Z (2010) Characteristics of the atmospheric water vapor and its relationship with rainfall in South China in northern autumn, winter and spring. J Trop Meteorol 26(5):626–632 **(Chinese)**

Liebmann B, Smith C (1996) Description of a complete (interpolated) outgoing longwave radiation dataset. Bull Am Meteorol Soc 77(6):1275–1277

Liu Y, Xu H, Lei Z (2009) Possible causes for drought in Sichuan-Chongqing region in summer 2006. Trans Atmos Sci 32(5):686–694 **(Chinese)**

Lv J, Ju J, Ren J et al (2012) The influence of the Madden-Julian Oscillation activity anomalies on Yunnan's extreme drought of 2009-2010. Sci China Earth Sci 55(1):98–112 **(Chinese)**

Matsumoto J, Murakami T (2002) Seasonal migration of monsoons between the Northern and Southern Hemisphere as revealed from equatorially symmetric and asymmetric OLR data. J Meteorol Soc Jpn 80(3):419–437

Matsumoto J, Murakami T, Jun M et al (2000) Annual changes of tropical convective activities as revealed from equatorial symmetric OLR data. J Meteorol Soc Jpn 78(5):543–561

McBride J (1998) Indonesia, Papua New Guinea, and tropical Australia, the southern hemisphere monsoon. Meteorology of the Southern Hemisphere. Am Meteorol Soc 49:89–99

McBride J, Haylock M, Nicholls N (2003) Relationships between the Maritime Continent heat source and the El Nin˜o–Southern Oscillation phenomenon. J Clim 16:2905–2914

Meehl G (1987) The annual cycle and interannual variability in the tropical Pacific and Indian Ocean regions. Mon Weather Rev 115(1):27–50

Neale R, Slingo J (2003) The Maritime Continent and its role in the global climate, A GCM Study. J Clim 16:834–848

Nitta Tsuyoshi (1987) Convective activities in the tropical western Pacific and their impact on the Northern Hemisphere summer circulation. J Meteorol Soc Jpn 65(3):373–390

Pal JS, Small EE, Eltahir E (2000) Simulation of regional-scale water and energy budgets: representation of subgrid cloud and precipitation processes within RegCM. J Geophys Res Atmos 105(D24):29579–29594

Qi D, Li Y, Li Y et al (2010) Variation of atmospheric heat source over east of the T-P in summer and its influence on climate of surrounding region. J Arid Meteor 28(2):113–120 **(Chinese)**

Qian D, Guan Z, Tang W (2018) Joint Impacts of SSTA in tropical Pacific and Indian Oceans on Variations of WPSH. J Meteorol Res 32(4):548–559

Ramage CS (1968) Role of a tropical "Maritime Continent" In the atmospheric circulation. Mon Weather Rev 96(6):365–370

Reynolds RW, Rayner NA, Smith TM et al (2002) An improved in situ and satellite SST analysis for climate. J Clim 15:1609–1625

Ropelewski CF, Halpert MS (1987) Global and regional scale precipitation patterns associated with the El Nino/Southern Oscillation. Mon Weather Rev 115:1606–1626

Saji NH, Goswami BN, Vinayachandran PN et al (1999) A dipole mode in the tropical Indian ocean. Nature 401(6751):360–363

Sardeshmukh PD, Hoskins BJ (1988) The generation of global rotational flow by steady, 598 idealized tropical divergence. J Atmos Sci 45:1228–1251

Sardeshmukh PD, Compo GP, Penland C (2000) Changes of probability associated with El Niño. J Clim 13:4268–4286

Song D, Guan Z, Tang W (2011) Variations of OLR in Maritime Continent regions in association with droughts and floods in the upper and middle reaches of Yangtze River of China in boreal summer. J Trop Meteorol 27(4):560–568 **(Chinese)**

Takaya K (2001) A formulation of a phase-independent wave-activity flux for stationary and migratory quasi-geostrophic eddies on a zonally varying basic flow. J Atmos Sci 58(6):608–627

Takaya K, Nakamura H (1997) A formulation of a wave-activity flux for stationary Rossby waves on a zonally varying basic flow. Geophys Res Lett 24(23):2985–2988

Tao S, Chen L (1987) A review of recent research on the East Asian summer monsoon in China. Monsoon Meteorology. Oxford University Press, London, pp 60–92

Tao S, Zhu F (1964) The 100-Mb flow patterns in Southern Asia in summer and its relation to the advance and retreat of the West Pacific subtropical anticyclone over the far east. Acta Meteorol Sin 34(4):385–396 **(Chinese)**

Wang B, Li Y (2010) Relationship analysis between south branch trough and severe drought of Southwest China during autumn and winter 2009/2010. Plateau Mt Meteor Res 30(4):26–35 **(Chinese)**

Wang B, Lin H (2002) Rainy season of the Asian–Pacific summer monsoon. J Clim 15(4):386–398

Wang XM, Zhou SW, Zhou B (2012) Causative analysis of continuous drought in Southwest China from autumn 2009 to Spring 2010. Meteorol Month 38(11):1399–1407

Wang J, Wen Z, Wu R et al (2016) The mechanism of growth of the low-frequency East Asia-Pacific teleconnection and the triggering role of tropical intraseasonal oscillation. Clim Dyn 46(11):3965–3977

Wang M, Guan Z, Jin D (2017) Two new sea surface temperature anomalies indices for capturing the eastern and central equatorial Pacific type El Niño-Southern Oscillation events during boreal summer. Int J Climatol 2018:1–11

Xia Y, Guan Z, Sun Y (2015) Interannual variations of OLR in maritime continent in late autumn and early winter and their relationships with precipitation anomalies over Yunnan-Kweichow Plateau. Acta Meteorol Sin 73(4):725–736 **(Chinese)**

Xia Y, Wan X, Yan X et al (2016) Variations of spring precipitation over Southwest China and circulation characteristics about its anomaly. Acta Meteorol Sin 74(4):510–524 **(Chinese)**

Xu Q, Guan Z (2017) Interannual variability of summertime outgoing longwave radiation over the Maritime Continent in relation to East Asian summer monsoon anomalies. J Meteorol Res 31(4):35–47

Xu Q, Guan Z, Jin D, Hu D (2019) Regional characteristics of interannual variability of summer rainfall in the Maritime Continent and their related anomalous circulation patterns. J Clim 32:4179–4192. https://doi.org/10.1175/JCLI-D-18-0480.1

Yang S, Lau KM, Kim KM (2002) Variations of the East Asian jet stream and Asian–Pacific–American winter climate anomalies. J. Clim 15:306–325

Yang J, Wang C, Lei Y (2013) Development and structure characteristic of southwest heat low in spring. Meteor Mon 39(2):146–155 **(Chinese)**

Zeng X, Zhao M, Dickinson RE (1998) Inter-comparison of bulk aerodynamic algorithms for the computation of sea surface fluxes using TOGA-coare and TAO data. J Clim 11:2628–2644

Zhang C, Hagos SM (2009) Bi–modal structure and variability of large-scale diabatic heating in the tropics. J Atmos Sci 66(12):3621–3640

Zhang W, Jin F, Zhao J et al (2013) The possible influence of a non-conventional el niño on the severe autumn drought of 2009 in southwest china. J Clim 26(21):8392–8405

Zhang Y, Fan G, Zhou D (2014) Variation of springtime southern branch trough and its relationship with precipitation and atmospheric circulation. Plateau Meteor 33(1):97–105 **(Chinese)**